

Probing the superconducting ground state of noncentrosymmetric high entropy alloys using muon-spin rotation and relaxation

Kapil Motla,¹ Arushi,¹ P. K. Meena,¹ D. Singh,² P. K. Biswas,² A. D. Hillier,² and R. P. Singh^{1,*}

¹*Department of Physics, Indian Institute of Science Education and Research Bhopal, Bhopal, 462066, India*

²*ISIS Facility, STFC Rutherford Appleton Laboratory,*

Harwell Science and Innovation Campus, Oxfordshire, OX11 0QX, UK

(Dated: September 9, 2021)

Recently, high entropy alloys (HEAs) have emerged as a new platform for discovering superconducting materials and offer avenues to explore exotic superconductivity. The highly disordered nature of HEA suggests regular phonon required for BCS superconductivity may be unlikely to occur. Therefore understanding the microscopic properties of these superconducting HEA is important. We report the first detailed characterization of the superconducting properties of the noncentrosymmetric (α -Mn structure) HEA (HfNb)_{0.10}(MoReRu)_{0.90}, and (ZrNb)_{0.10}(MoReRu)_{0.90} by using magnetization, specific heat, AC transport, and muon-spin relaxation/rotation (μ SR). Despite the disordered nature, low temperature specific heat and transverse-field muon spin rotation measurements suggest nodeless isotropic superconducting gap and Zero-field μ SR measurements confirm that time reversal symmetry is preserved in the superconducting ground state.

I. INTRODUCTION

High entropy alloys (HEAs) are a new class of materials with tunable physical and superior mechanical properties compared to conventional binary and ternary alloys. These materials are getting widespread attention from many different scientific areas, material science, theoretical and experimental condensed matter physics [1–6]. HEA are multi-component alloys that contain five or more elements in near equimolar ratios [7–10]. The Gibbs free energy decreases at high temperature and plays a vital role in crystallizing HEA in different crystallographic structures [2, 11, 12]. Recently, HEA has emerged as a new class of disordered alloy superconductors, having a high superconducting transition temperature and critical field. Also, it shows retention of superconductivity at very high pressure [13]. Superconductivity was first reported in the high entropy alloy, Ta₃₄Nb₃₃Hf₈Zr₁₄Ti₁₁ [14], since then it has been observed in a few others high entropy alloys [15–18, 20–22]. To date, most of the research in HEA superconductors has been focused on discovering new HEA superconducting materials that crystallises in various structures and enhancing the superconducting transition temperature. In contrast, the superconducting pairing mechanism is largely unexplored, mainly due to the HEA multi-component and a high disorder nature. It is difficult to calculate the electronic structure and understand the lattice vibration, which is usually essential for understanding the superconducting pairing mechanism. A comparative study with binary alloy superconductors with HEA, which have the same crystal structure and a large disorder, can provide more insight into the

superconducting properties of HEA. A topical example of a binary alloy is the Re-based superconductors. These materials have a noncentrosymmetric α -Mn crystal structure and have been studied extensively due to the presence of time-reversal symmetry (TRS) breaking [23–27]. However, the exact superconducting pairing mechanism is still not fully understood. Structural similarity, disorder, and the multi-component nature of Re-based noncentrosymmetric (NCS) HEA, may help understand the superconducting pairing mechanism of noncentrosymmetric superconducting compounds and HEA itself, which is still elusive. In this paper, we have performed a comprehensive study superconducting ground state, using magnetization, heat capacity, and resistivity, together with muon-spin spectroscopy on a new NCS α -Mn HEA (HfNb)_{0.10}(MoReRu)_{0.90} having a $T_C = 5.9(1)$ K and another α -Mn NCS HEA (ZrNb)_{0.10}(MoReRu)_{0.90} reported by Stolze et al. [18]) having a T_C 5.8(1) K.

II. EXPERIMENTAL DETAILS

Polycrystalline samples of (HfNb)_{0.10}(MoReRu)_{0.90} and (ZrNb)_{0.10}(MoReRu)_{0.90} HEA were prepared by arc-melting stoichiometric quantities of high-purity elements (5N) under argon (5N) atmosphere. The resulting ingots were flipped and melted several times to enhance the homogeneity. In both HEAs, the weight loss was negligible (< 0.1%) after melting. Phase purity and crystal structure of the samples were confirmed by X-ray diffraction (XRD) at room temperature on a PANalytical diffractometer equipped with CuK_α radiation ($\lambda = 1.54056$ Å).

Temperature and field dependent magnetization, heat capacity and transport measurements were performed

* rpsingh@iiserb.ac.in

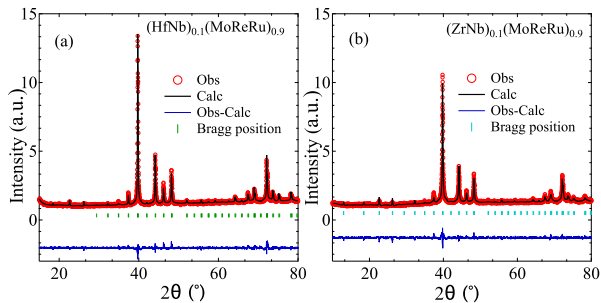


FIG. 1. Color online: The X-ray diffraction pattern from $(\text{HfNb})_{0.10}(\text{MoReRu})_{0.90}$ (left) and $(\text{ZrNb})_{0.10}(\text{MoReRu})_{0.90}$ (right) collected at room temperature using $\text{CuK}\alpha$ radiation ($\lambda = 1.54056 \text{ \AA}$). The black line is the Le Bail fitting and the green dashes are the expected locations for the diffraction Bragg peaks.

using a Quantum Design, MPMS-3 and PPMS. The μSR measurements in zero-field (ZF) and transverse-field (TF) conditions were carried out using the MUSR spectrometer at the ISIS Neutron and Muon Facility, STFC Rutherford Appleton Laboratory, United Kingdom. A full description of the μSR technique may be found in Ref. [28].

III. RESULTS

a. Structural characterization

X-ray diffraction spectra from both HEA were collected at ambient conditions and Le Bail fitting using the Fullprof software [29] as shown in Fig. 1. This shows that both alloys crystallize in a cubic non-centrosymmetric $\alpha\text{-Mn}$ (space group $\text{I}\bar{4}3m$) crystal structure and have unit cell parameters: $a = 9.6170(2) \text{ \AA}$ and $9.6180(2) \text{ \AA}$ for $(\text{HfNb})_{0.10}(\text{MoReRu})_{0.90}$ and $(\text{ZrNb})_{0.10}(\text{MoReRu})_{0.90}$ respectively. The refined cell parameters of $(\text{ZrNb})_{0.10}(\text{MoReRu})_{0.90}$ are in good agreement with the published data [18]. Due to large number of different atoms/sites and tendency to form solid solution makes difficult to determine the occupancies of atomic sites unambiguously (See supplementary information [19]).

b. Normal and superconducting state properties

1. Electrical Resistivity

Temperature dependence of the resistivity, $\rho(T)$, for both samples were performed in zero field from 1.9 K to 300 K. The results for $(\text{HfNb})_{0.10}(\text{MoReRu})_{0.90}$ and $(\text{ZrNb})_{0.10}(\text{MoReRu})_{0.90}$ are shown in Fig. 2(a) and 2(b) respectively. Low temperature data is shown in the top inset of Fig. 2(a) and Fig. 2(b) clearly

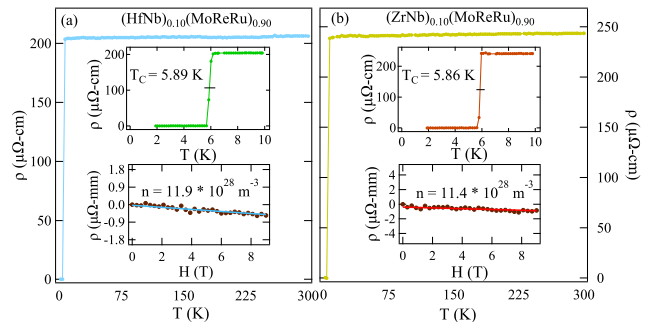


FIG. 2. Temperature dependence of the resistivity for a) $(\text{HfNb})_{0.10}(\text{MoReRu})_{0.90}$, b) $(\text{ZrNb})_{0.10}(\text{MoReRu})_{0.90}$ in zero field. The top of both Insets is showing the superconducting transition and the bottom of both insets is showing the field-dependent hall resistivity at 10 K.

presents a very sharp drop in resistivity at $T_C^{\text{mid}} = 5.9(1) \text{ K}$ and $5.8(1) \text{ K}$ for $(\text{HfNb})_{0.10}(\text{MoReRu})_{0.90}$ and $(\text{ZrNb})_{0.10}(\text{MoReRu})_{0.90}$, respectively. Resistivity increases leisurely with temperature showing poor metallic behavior. The residual resistivity ratio (RRR) for both the samples found to be 1.2. The small value of RRR for both HEAs indicates a high degree of disorder and these values are comparable to reported RRR ratio for HEAs and $\alpha\text{-Mn}$ binary alloys [18, 24–26, 30]. Hall measurement was also performed to calculate the carrier concentration and the type of charge carriers. Lower inset in Fig. 2(a) and 2(b) shows the field dependence of hall resistivity (ρ) measured at $T = 10 \text{ K}$ for both HEA's. $\rho(H)$ is well described by a straight line fit and carrier concentration yields $n = 11.9(4) \times 10^{-28} \text{ m}^{-3}$ and $11.4(8) \times 10^{-28} \text{ m}^{-3}$ respectively for $(\text{HfNb})_{0.10}(\text{MoReRu})_{0.90}$ and $(\text{ZrNb})_{0.10}(\text{MoReRu})_{0.90}$.

2. Magnetization

To confirm bulk superconductivity in both HEA, the temperature dependence of the DC magnetization measurements were performed in an applied field of 1.0 mT in zero field cooled warming (ZFCW) and field cooled cooling (FCC) modes. The onset of superconductivity was observed below $T_C = 5.2(1) \text{ K}$ for $(\text{HfNb})_{0.10}(\text{MoReRu})_{0.90}$ and $5.5(1) \text{ K}$ for $(\text{ZrNb})_{0.10}(\text{MoReRu})_{0.90}$ by a sharp decrease in a diamagnetic magnetisation, as shown in Fig. 3(a) and 3(e). In order, to estimate the lower critical field H_{C1} , we have performed magnetization versus field measurements at a range of temperatures. The value of the H_{C1} at each temperature is taken as the deviation of the magnetisation from the linearity, as shown in the inset of Fig. 3(b) and 3(f) for $(\text{HfNb})_{0.10}(\text{MoReRu})_{0.90}$ and $(\text{ZrNb})_{0.10}(\text{MoReRu})_{0.90}$. The lower critical field at absolute zero temperature, $H_{C1}(0)$ can be calculated by extrapolating $H_{C1}(T)$ using the Ginzburg-Landau

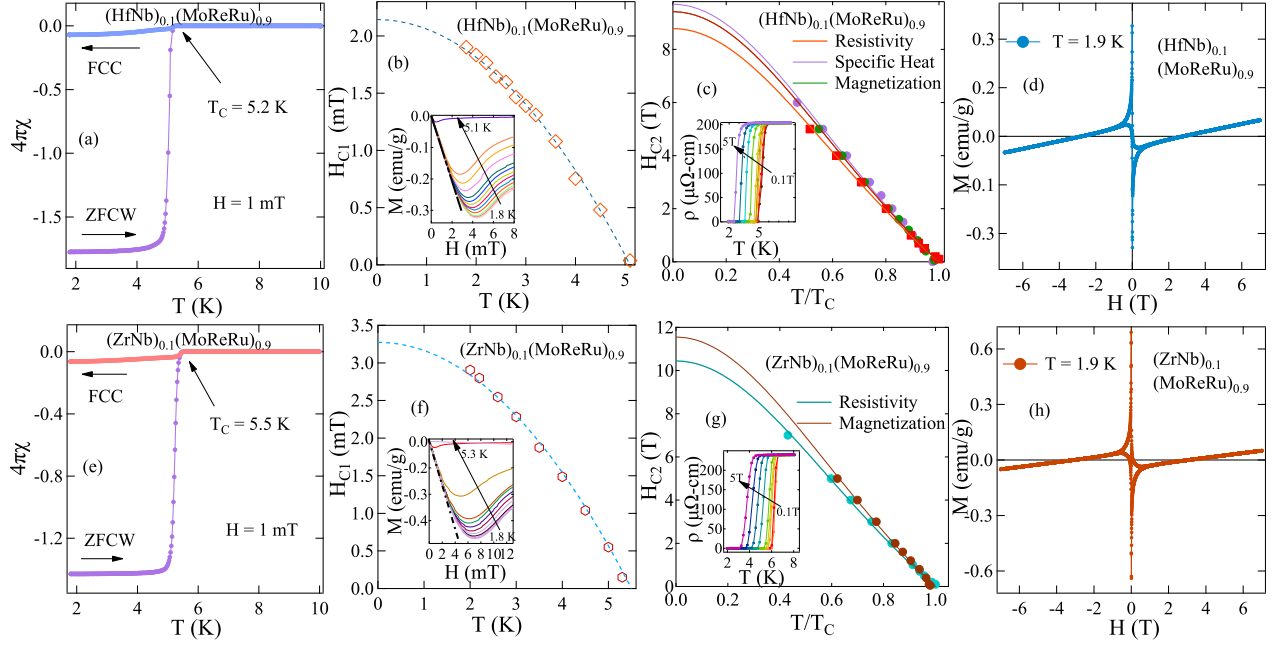


FIG. 3. (a) and (e) show the temperature dependence of magnetic moment in 1.0 mT in FCC and ZFCW mode. (b) and (f) show the temperature dependence of lower critical field. (c) and (g) show the upper critical field estimated using specific heat, resistivity, and magnetization data. The dotted lines is the result of the fit to equation 2. (d) and (h) Magnetic field dependent magnetization (M-H) at 1.9 K.

expression, which is given as

$$H_{C1}(T) = H_{C1}(0) (1 - t^2) \quad (1)$$

where $t = T/T_C$, and lower critical field $H_{C1}(0)$ was estimated as 2.14(1) mT and 3.27(3) mT for (HfNb)_{0.10}(MoReRu)_{0.90} and (ZrNb)_{0.10}(MoReRu)_{0.90} respectively by fitting the Eq. 1 in the data given in Fig. 3(b) and 3 (f).

The upper critical field at $T = 0$ K, $H_{C2}(0)$ estimated using Ginzburg-Landau (GL) relation

$$H_{C2}(T) = H_{C2}(0) \left(\frac{1 - t^2}{1 + t^2} \right) \quad (2)$$

where $t = T/T_C$, and the estimated value of $H_{C2(res,mag,hc)}(0) = 8.7(1)$ T, $9.4(1)$ T, $9.7(1)$ T for (HfNb)_{0.10}(MoReRu)_{0.90} and $H_{C2(Res,mag)}(0) = 10.4(9)$ T, $11.5(2)$ T for (ZrNb)_{0.10}(MoReRu)_{0.90}. The Ginzburg-Landau coherence length (the length between cooper pair) can be estimated with the help of $H_{C2}(0)$ by using the expression

$$H_{C2}(0) = \frac{\Phi_0}{2\pi\xi_{GL}^2} \quad (3)$$

where Φ_0 is the flux quantum ($\Phi_0 = 2.07 \times 10^{-15} \text{T}\cdot\text{m}^2$). After substituting $H_{C2}(0)$ value from magnetization gives $\xi_{GL} = 5.92(2)$ nm for (HfNb)_{0.10}(MoReRu)_{0.90}

and 5.35(3) nm for (ZrNb)_{0.10}(MoReRu)_{0.90}. The calculated values of $H_{C1}(0)$ and $\xi_{GL}(0)$ were used to evaluate magnetic penetration depth $\lambda_{GL}(0)$ (the value of distance at which magnetic field become $1/e$ times of external applied magnetic field) for both the samples with the help of relation

$$H_{C1}(0) = \frac{\Phi_0}{4\pi\lambda_{GL}^2(0)} \left(\ln \frac{\lambda_{GL}(0)}{\xi_{GL}(0)} + 0.12 \right) \quad (4)$$

and were obtained as 609(2) nm and 487(3) nm for (HfNb)_{0.10}(MoReRu)_{0.90} and (ZrNb)_{0.10}(MoReRu)_{0.90} respectively. Ginzburg-Landau ratio is given by $\frac{\lambda_{GL}(0)}{\xi_{GL}(0)}$, $\kappa_{GL} > \frac{1}{\sqrt{2}}$ for (HfNb)_{0.10}(MoReRu)_{0.90} and (ZrNb)_{0.10}(MoReRu)_{0.90} respectively. This confirms that both of these HEA are indeed strong type II superconductors.

In a type-II superconductor, Cooper pair breaking due to the applied magnetic field is attributed to two types of mechanisms: orbital limiting field and Pauli paramagnetic limiting field effect [31, 32]. In the orbital pair breaking, the induced kinetic energy of a Cooper pair by an external field exceeds to the Cooper pair condensation energy. Whereas in Pauli limiting, the applied magnetic field aligns one of the Cooper pair spin moments in the direction of its field, thereby breaking the pairing. Orbital limiting field, $H_{C2}^{orbital}(0)$ is given by the Werthamer-Helfand-Hohenberg (WHH) expression

$$H_{C_2}^{orbital}(0) = -\alpha T_C \left. \frac{dH_{C_2}(T)}{dT} \right|_{T=T_C} \quad (5)$$

where α is purity factor and 0.693 value define for dirty limit superconductors (see discussion section). The initial slope $-\frac{dH_{C_2}}{dT}$ at $T = T_C$ were estimated 2.24(5) T/K , and 2.6(2) T/K for $(\text{HfNb})_{0.10}(\text{MoReRu})_{0.90}$, and $(\text{ZrNb})_{0.10}(\text{MoReRu})_{0.90}$ respectively, and gives the orbital limiting upper critical field $H_{C_2}^{orb}(0)$ as 8.0(2) T for $(\text{HfNb})_{0.10}(\text{MoReRu})_{0.90}$ and 9.9(5) T for $(\text{ZrNb})_{0.10}(\text{MoReRu})_{0.90}$. The Pauli paramagnetic limit is given by $H_{C_2}^P = 1.84 T_C$ within the BCS theory. Substituting the values of T_C , we have determined $H_{C_2}^P = 9.56(2)$ and $10.12(2)$ T for $(\text{HfNb})_{0.10}(\text{MoReRu})_{0.90}$, and $(\text{ZrNb})_{0.10}(\text{MoReRu})_{0.90}$ respectively. The Maki parameter, which is a measure of the strength of Pauli limiting field and orbital critical field is given by the expression $\alpha_M = \sqrt{2}H_{C_2}^{orb}(0)/H_{C_2}^P(0)$. The values obtained for α_M are 1.18 for $(\text{HfNb})_{0.10}(\text{MoReRu})_{0.90}$ and 1.38 for $(\text{ZrNb})_{0.10}(\text{MoReRu})_{0.90}$.

The magnetization hysteresis loops (± 9.0 T) for both HEAs at 1.9 K is shown in Fig. 3(d) and 3(h). A closed-loop form at 2.0 T and 3.5 T , denotes the H_{irr} is far below from their upper critical magnetic fields of both HEA samples. These values of H_{irr} is suggesting the depinning of the flux line vortexes. The depinning generally happens due to the thermal fluctuation on the condensation energy of Cooper pair or stress induced by grain boundary/disorder in polycrystalline samples. The strength of thermal fluctuation with respect to condensation energy of charge carriers is described by the G_i number [33]. The calculated value of G_i for both HEAs ($\sim 10^{-5}$) and falls between high T_C ($\sim 10^{-2}$) and conventional superconductors ($\sim 10^{-8}$), suggesting the defect and grain boundaries can be responsible for depinning [34].

3. Specific Heat

Specific heat measurement for both samples were performed between 1.9 - 20 K in zero-field. The observed T_C for both the samples is in agreement with the magnetization and resistivity data. The specific heat data above T_C in the normal region was fitted using the equation: $\frac{C}{T} = \gamma_n + \beta_3 T^2 + \beta_5 T^4$ and is shown in the insets of Fig. 4. Here γ_n is the coefficient for electronic specific heat in the normal state (Sommerfeld coefficient) and β_3 and β_5 are the phononic contribution. The fitting provides the parameters as: $\gamma_n = (3.6(1), 3.8(1))$ $mJ\text{-mol}^{-1}K^{-2}$, $\beta_3 = (0.047(1), 0.052(3))$ $mJ\text{-mol}^{-1}K^{-4}$, and $\beta_5 = (0.07(1), 0.07(1))$ $\mu J\text{-mol}^{-1}K^{-6}$ for $(\text{HfNb})_{0.10}(\text{MoReRu})_{0.90}$, $(\text{ZrNb})_{0.10}(\text{MoReRu})_{0.90}$ respectively.

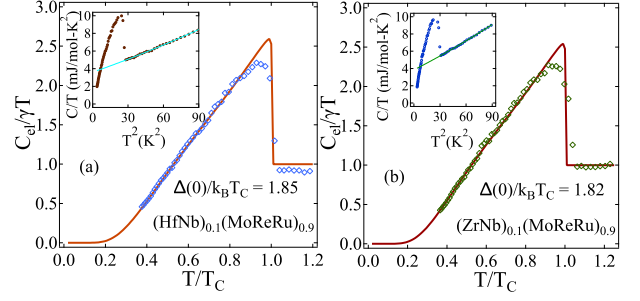


FIG. 4. Normalised specific heat data $C_{el}/\gamma_n T$ fitted with the BCS s -wave model shown by the red line for both HEAs (a) $(\text{HfNb})_{0.10}(\text{MoReRu})_{0.90}$ and (b) $(\text{ZrNb})_{0.10}(\text{MoReRu})_{0.90}$. The inset shows the temperature dependent specific heat data in zero field data plotted as C/T vs T^2 .

The density of state $D_C(E_F)$ and Debye temperature, θ_D have been calculated using γ_n and β_3 . The obtained value of $D_C(E_F) = (1.53(3), 1.63(4)) \frac{\text{states}}{eV f.u}$ and $\theta_D = 346(2)$ K , $335(7)$ K for $(\text{HfNb})_{0.10}(\text{MoReRu})_{0.90}$, $(\text{ZrNb})_{0.10}(\text{MoReRu})_{0.90}$ respectively. Moreover, the strength of the attractive interaction between electron and phonon can be expressed according to the McMillan model [35] as

$$\lambda_{e-ph} = \frac{1.04 + \mu^* \ln(\theta_D/1.45 T_C)}{(1 - 0.62 \mu^*) \ln(\theta_D/1.45 T_C) - 1.04} \quad (6)$$

here μ^* is the screened Coulomb repulsion parameter which is usually between 0.1-0.15 and for inter-metallic superconductors ~ 0.13 [25, 26]. Inserting the value of Debye temperature, θ_D and T_C , we find the strength between electron and phonon, $\lambda_{e-ph} = 0.62(6)$ and $0.63(8)$ for $(\text{HfNb})_{0.10}(\text{MoReRu})_{0.90}$ and $(\text{ZrNb})_{0.10}(\text{MoReRu})_{0.90}$ respectively. This value indicates a moderately coupled superconductivity similar to other Re based noncentrosymmetric superconductors such as Re_6Hf [25] and $\text{Re}_{24}\text{Ti}_5$ [36].

In order to determine the electronic specific heat contribution, we have subtracted the phononic contribution from the total specific heat: $C_{el} = C(T) - \beta_3 T^3 - \beta_5 T^5$. The normalized electronic specific heat jump, $\frac{\Delta C_{el}}{\gamma_n T_C} = 1.67$ for $(\text{HfNb})_{0.10}(\text{MoReRu})_{0.90}$ and 1.49 for $(\text{ZrNb})_{0.10}(\text{MoReRu})_{0.90}$ which further suggests moderately coupled superconductivity for both these HEA samples. The electronic specific heat data below transition temperature T_C can be best fitted with single-gap BCS expression for normalized entropy, S

$$\frac{S}{\gamma_n T_C} = -\frac{6}{\pi^2} \left(\frac{\Delta(0)}{k_B T_C} \right) \int_0^{\infty} [f \ln(f) + (1-f) \ln(1-f)] dy \quad (7)$$

where $f(\xi) = [\exp(E(\xi)/k_B T) + 1]^{-1}$ is the Fermi function, $E(\xi) = \sqrt{\xi^2 + \Delta^2(t)}$, where $E(\xi)$ is the energy of

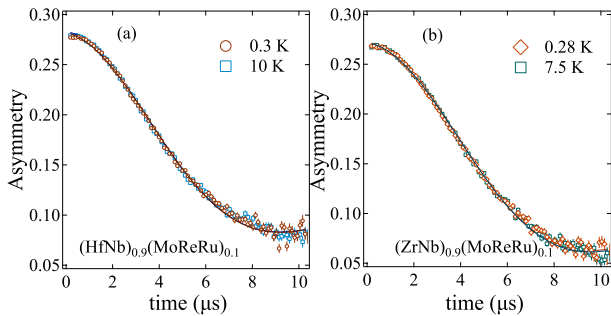


FIG. 5. Temperature dependent ZF- μ SR asymmetry spectra collected above and below the transition temperature for both the samples. The fitting curve is shown as solid red curve.

the normal electrons relative to the Fermi energy, $y = \xi/\Delta(0)$, $t = T/T_C$ and $\Delta(t) = \tanh[1.82(1.018((1/t)-1))^{0.51}]$ is the BCS approximation for the temperature dependence of the energy gap. The normalized electronic specific heat below T_C is related to the normalized entropy by

$$\frac{C_{el}}{\gamma_n T_C} = t \frac{d(S/\gamma_n T_C)}{dt} \quad (8)$$

Fig. 4 shows the Eq. 8 fits to the specific heat data. This provides $\frac{\Delta(0)}{k_B T_C} = 1.85(3)$ and $1.82(2)$ for $(\text{HfNb})_{0.10}(\text{MoReRu})_{0.90}$, $(\text{ZrNb})_{0.10}(\text{MoReRu})_{0.90}$ respectively, both of which are higher than the usual BCS value in the weak coupling limit, again suggesting moderately coupled superconductivity in both HEA's.

4. Muon spin relaxation and rotation

The nature of superconducting ground state of both HEAs, $(\text{HfNb})_{0.10}(\text{MoReRu})_{0.90}$ and $(\text{ZrNb})_{0.10}(\text{MoReRu})_{0.90}$ was further investigated by using muon spin relaxation and rotation measurements. First, we shall discuss the ZF- μ SR measurements, which were carried out above and below T_C for both samples. This was to detect any possibility of the presence of time reversal symmetry breaking signal. The absence of any precession signal confirms the absence of local magnetic field associated with long-range ordering, and depolarization of muon spin occurs due to the presence of static randomly oriented nuclear moments. In the absence of magnetic moment, the behavior of time-dependent muon asymmetry spectra is best described by Gaussian Kubo-Toyabe function [37]

$$G_{\text{KT}}(t) = \frac{1}{3} + \frac{2}{3}(1 - \sigma_{\text{ZF}}^2 t^2) \exp\left(\frac{-\sigma_{\text{ZF}}^2 t^2}{2}\right) \quad (9)$$

where σ_{ZF} is the relaxation rate of muon-spin due to

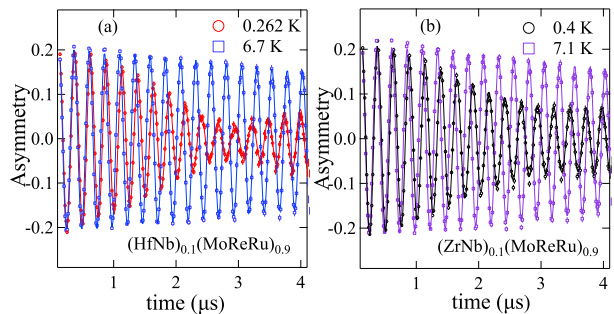


FIG. 6. Transverse field asymmetry spectra were collected at 30 mT magnetic field above and below the transition temperature of HEAs. The solid line is the fit which using the a Gaussian modulated oscillatory function.

static, randomly oriented local fields associated with the nuclear moments. The time-dependent asymmetry spectra can be best described by the following function

$$A(t) = A_1 G_{\text{KT}}(t) \exp(-\Lambda t) + A_{\text{BG}} \quad (10)$$

where A_1 and A_{BG} are the sample asymmetry and non-decaying constant background signal while Λ is an electronic relaxation rate. ZF- μ SR spectra collected both in normal and superconducting state exhibit the identical relaxations can be seen in overlapping ZF- μ SR spectra (Fig. 5). It confirms additional ZF- μ SR relaxations below superconducting transition temperature exclude the possibility of time reversal symmetry in superconducting ground state of both the HEA's.

To gain information on the superconducting gap structure, we have performed TF- μ SR measurement where an applied magnetic field of 30 mT was applied above the superconducting transition temperature, and then the sample was cooled to the base temperature 0.26 K of the He^3 cryostat. The applied magnetic field is greater than H_{C1} but less than H_{C2} in order to generate a flux line lattice. Fig. 6 shows the TF- μ SR asymmetry spectra below and above T_C for both HEAs. The fast decay of TF- μ SR spectra below T_C with respect to above T_C spectra is due to the formation of flux lattice line. The TF- μ SR signal is best fitted with the oscillatory function:

$$A(t) = \sum_{i=1}^N A_i \exp\left(-\frac{1}{2}\sigma_i^2 t^2\right) \cos(\gamma_\mu B_i t + \phi) + A_{bg} \cos(\gamma_\mu B_{bg} t + \phi) \quad (11)$$

where B_i is mean field of the i_{th} component of the Gaussian distribution, B_{bg} is the contribution from the sample holder, A_i and A_{bg} are the asymmetry contribution from the sample and sample holder, ϕ is the initial phase offset, and σ is the Gaussian muon spin depolarization rate. The second moment was used in case of $(\text{HfNb})_{0.10}(\text{MoReRu})_{0.90}$ and the first and second

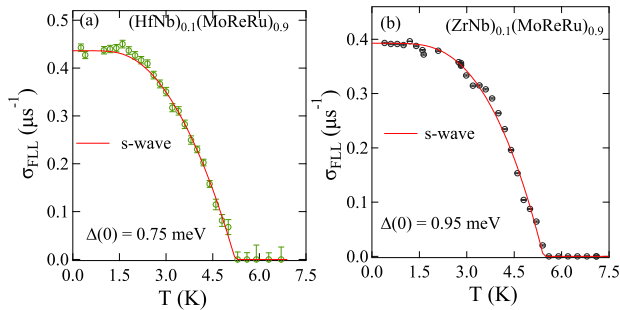


FIG. 7. TF field muon depolarization data collected at 30 mT . The data is well described using an isotropic s -wave model for both $(\text{HfNb})_{0.10}(\text{MoReRu})_{0.90}$ (left) and $(\text{ZrNb})_{0.10}(\text{MoReRu})_{0.90}$ (right).

moments are given as

$$B = \sum_{i=1}^2 \frac{A_i B_i}{A_1 + A_2}, \quad (12)$$

$$\langle \Delta B^2 \rangle = \frac{\sigma^2}{\gamma_\mu^2} = \sum_{i=1}^2 \frac{A_i [(\sigma_i/\gamma_\mu)^2 + (B_i - B)^2]}{A_1 + A_2} \quad (13)$$

σ includes both the temperature-independent depolarization, σ_N , which is coming from the static field arises due to the nuclear magnetic moment and the contribution of the field variation from the flux line lattice and is given as $\sigma^2 = \sigma_N^2 + \sigma_{FLL}^2$. As for both the samples, $\xi(0)/l > 1$ (see Table 1), temperature dependent London magnetic penetration depth in dirty limit within London approximation, can be estimated by following expression

$$\frac{\sigma_{FLL}(T)}{\sigma_{FLL}(0)} = \frac{\lambda^{-2}(T)}{\lambda^{-2}(0)} = \frac{\Delta(T)}{\Delta(0)} \tanh \left[\frac{\Delta(T)}{2k_B T} \right] \quad (14)$$

The solid line in Fig. 7 is the fit using Eq. (14) to the muon depolarisation rate from the flux line lattice which reveals the values of energy gap as $\Delta(0) = 0.75(3) \text{ meV}$ ($\Delta(0)/k_B T_C = 1.68(6)$) for $(\text{HfNb})_{0.10}(\text{MoReRu})_{0.90}$ and $\Delta(0) = 0.95(1) \text{ meV}$ ($\Delta(0)/k_B T_C = 1.96(8)$) for $(\text{ZrNb})_{0.10}(\text{MoReRu})_{0.90}$. These values are in good agreement with the values obtained from specific heat data. For high $H_{c2}(0)$ superconductor, muon spin relaxation rate in the superconducting state (σ_{FLL}) is related to London penetration depth λ via expression [38, 39];

$$\frac{\sigma_{FLL}(T)}{\gamma_\mu^2} = \frac{0.00371 \Phi_0^2}{\lambda^4(T)} \quad (15)$$

where $\gamma_\mu/2\pi = 135.5 \text{ MHz}/T$ is muon gyromagnetic ratio and Φ_0 is the magnetic flux quantum. Within the

London approximation, the estimated value of $\lambda(0)$ are 495(6) nm and 522(1) nm for $(\text{HfNb})_{0.10}(\text{MoReRu})_{0.90}$ and $(\text{ZrNb})_{0.10}(\text{MoReRu})_{0.90}$, respectively.

5. Discussions

To supplement the results of the experimental measurements, we have performed calculations of the electronic properties. The electronic heat coefficient γ_n is directly dependent on effective mass m^* and carrier density n of quasi-particle via this expression [40].

$$\gamma_n = \left(\frac{\pi}{3} \right)^{2/3} \frac{k_B^2 m^* n^{1/3}}{\hbar^2} \quad (16)$$

where k_B is Boltzman constant, using the electronic heat coefficient $\gamma_n = 3.6(1)$ and $3.8(1) \text{ mJ-mol}^{-1}\text{K}^{-2}$ (determine from normal state heat capacity), and the carrier density $n = 11.9(4)$, $11.4(8) \times 10^{28} \text{ m}^{-3}$ (obtain by hall measurement) for $(\text{HfNb})_{0.10}(\text{MoReRu})_{0.90}$ and $(\text{ZrNb})_{0.10}(\text{MoReRu})_{0.90}$ respectively. This yield effective mass $m^* = 4.7(2) m_e$, and $5.3(2) m_e$ respectively for $(\text{HfNb})_{0.10}(\text{MoReRu})_{0.90}$ and $(\text{ZrNb})_{0.10}(\text{MoReRu})_{0.90}$. The carrier density n and effective mass m^* of quasi-particle are related to Fermi velocity v_F by the expression

$$n = \frac{1}{3\pi^2} \left(\frac{m^* v_f}{\hbar} \right)^3 \quad (17)$$

the expression give the Fermi velocity $v_F = 3.7(2)$, $3.2(2) \times 10^5 \text{ m/s}$ for $(\text{HfNb})_{0.10}(\text{MoReRu})_{0.90}$ and $(\text{ZrNb})_{0.10}(\text{MoReRu})_{0.90}$ respectively. The mean free path l is related to residual resistivity ρ_0 , effective mass m^* and Fermi velocity v_F of quasi-particle as;

$$l = \frac{3\pi^2 \hbar^3}{e^2 \rho_0 m^* v_F^2} \quad (18)$$

Using the previous calculated value of effective mass m^* , the Fermi velocity v_F with residual resistivity at transition temperature $\rho_0 = 204(1) \mu\Omega\text{-cm}$ and $238(1) \mu\Omega\text{-cm}$ (from resistivity measurement), we obtain the electronic mean free path $l = 2.6(2) \text{ \AA}$, and $2.4(5) \text{ \AA}$ for $(\text{HfNb})_{0.10}(\text{MoReRu})_{0.90}$ and $(\text{ZrNb})_{0.10}(\text{MoReRu})_{0.90}$, respectively. Within the BCS theory, the coherence length ξ_0 can be expressed in term of Fermi velocity v_F and transition temperature T_C as

$$\xi_0 = \frac{0.18 \hbar v_F}{k_B T_C} \quad (19)$$

here k_B is Boltzman constant, v_F and T_C (from magnetization) are the Fermi velocity and transition temperature, by which, we get $\xi_0 = 974(71) \text{ \AA}$, $797(64) \text{ \AA}$ and the ratio of $\xi_0/l > 1$ for both $(\text{HfNb})_{0.10}(\text{MoReRu})_{0.90}$ and $(\text{ZrNb})_{0.10}(\text{MoReRu})_{0.90}$, which is clearly suggesting the signature of dirty limit superconductivity for both

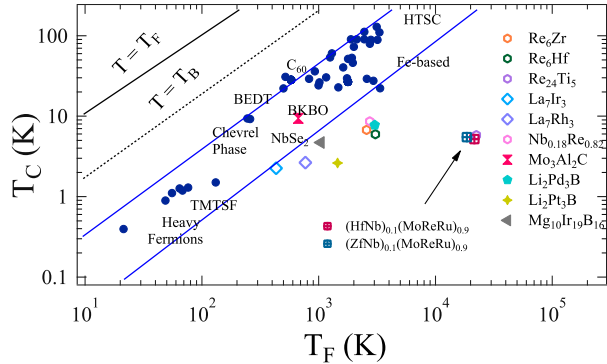


FIG. 8. A plot of superconducting transition temperature versus Fermi temperature for different superconducting families. Two solid blue lines show the unconventional band of superconductors with other exotic superconductors [44–47] and lies near the unconventional band. $(\text{HfNb})_{0.10}(\text{MoReRu})_{0.90}$ and $(\text{ZrNb})_{0.10}(\text{MoReRu})_{0.90}$ are shown by red and blue square symbol, which lie far from the other unconventional superconductors.

the HEA samples. The calculated parameter are listed in Table 1.

Uemura *et al.* [41–43] classified the superconductor in conventional and unconventional on behalf of the ratio of superconducting temperature to the Fermi temperature. If this ratio value falls between $0.01 \leq T_c/T_F \leq 0.1$, then a superconductor is considered as an unconventional one, and heavy fermion superconductor, high T_C superconductor, organic superconductor, Fe-based superconductor lie inside this band. To calculating the T_F value for both HEA samples, the expression used is as follows: $k_B T_F = \frac{\hbar^2}{2m^*} (3\pi^2 n)^{2/3}$ where m^* , k_B , and n are the effective mass, Boltzmann constant, and carrier density, respectively. The estimated value of T_F for $(\text{HfNb})_{0.10}(\text{MoReRu})_{0.90}$ and $(\text{ZrNb})_{0.10}(\text{MoReRu})_{0.90}$ are 21520(1480) K and 18589(1445) K. The T_C/T_F which are far from the boundary of the unconventional superconductor like the other noncentrosymmetric and unconventional superconductors.

IV. CONCLUSION AND SUMMARY

In conclusion, we have performed the first full characterisation of the superconducting properties on the NCS HEAs. In particular, $(\text{HfNb})_{0.10}(\text{MoReRu})_{0.90}$ and $(\text{ZrNb})_{0.10}(\text{MoReRu})_{0.90}$ by using μSR , magnetisation, transport and heat capacity measurements. This confirms bulk superconductivity and $H_{C2}(0)$ is close to the Pauli limiting field, like other Re-based NCS superconductors. The specific heat and TF- μSR measurements suggest moderately coupled superconductivity with the isotropic superconducting gap. The ZF- μSR result indicates time reversal symmetry is preserved in the superconducting ground state for both the HEAs. Comparing

TABLE I. Superconducting and normal state parameters of $(\text{HfNb})_{0.10}(\text{MoReRu})_{0.90}$ (Hf-HEA) and $(\text{ZrNb})_{0.10}(\text{MoReRu})_{0.90}$ (Zr-HEA)

PARAMETERS	UNIT	Hf-HEA	Zr-HEA
T_C	K	5.2(1)	5.5(1)
$H_{C1}(0)$	mT	2.1(1)	3.2(3)
$H_{C2}^{mag}(0)$	T	9.4(1)	11.5(2)
$H_{C2}^P(0)$	T	9.56(3)	10.12(3)
ξ_{GL}	nm	5.92(2)	5.35(3)
λ_{GL}	nm	609(2)	487(3)
$\lambda(0)_{muon}$	nm	495(6)	522(1)
k_{GL}		103(1)	91(1)
$\Delta_{C_{el}}/\gamma_n T_C$		1.67(5)	1.49(4)
$\Delta(0)/k_B T_C$ (specific heat)		1.85(3)	1.82(2)
$\Delta(0)/k_B T_C$ (muon)		1.68(6)	1.96(8)
m^*/m_e		4.7(2)	5.3(2)
v_F	10^5 m s^{-1}	3.7(2)	3.2(2)
n_s	10^{28} m^{-3}	11.9(4)	11.4(8)
ξ_0/l_e		374(98)	332(93)

the superconducting parameter of the NCS HEA with the binary Re-based compounds (except the preserved time reversal symmetry in the superconducting ground state) are surprisingly similar. The preserved TRS in the Re-based HEA's superconducting ground state despite structural and superconducting properties similarity with Re_6X series of compounds indicates the complex interplay of disorder and Re in the presence and absence of TRSB in the superconducting ground state. Similarity to binary superconductors and very low heat capacity value (in range of elements) in multicomponent HEA warrant further microscopic studies on more superconducting HEA to understand whether all superconducting HEA alloys show similar behaviour or HEA's with α -Mn crystal structure are unique.

V. ACKNOWLEDGMENTS

Kapil Motla acknowledges the Council of Scientific and Industrial Research (CSIR) Government of India for providing SRF fellowship (Award No. 09/1020(0123)/2017-EMR-I). R. P. S. acknowledge Science and Engineering Research Board, Government of India for the Core Research Grant CRG/2019/001028. We thank ISIS, STFC, UK for the beamtime to perform the μSR experiments [48].

-
- [1] M. -H. Tsai and J. -W. Yeh, *Mater. Res. Lett.* 2, 107 (2014).
- [2] Y. F. Ye, Q. Wang, J. Lu, C. T. Liu and Y. Yang, *Mat. Today* 19, 349 (2016).
- [3] Z. Li, K. G. Pradeep, Y. Deng, D. Raabe and C. C. Tasan, *Nature* 534, 227 (2016).
- [4] C. Lee, G. Song, M. C. Gao, R. Feng, P. Chen, J. Brechtel, Y. Chen, K. An, W. Guo, J. D. Poplawsky, S. Li, A. T. Samaei, W. Chen, A. Hu, H. Choo, P. K. Liaw, *Acta Materials*, 160, 158 (2018).
- [5] Z. Fan, H. Wang, Y. Wu, X. J. Liu and Z. P. Lu, *RSC Adv.* 6, 52164 (2016).
- [6] Y. Zhang, T. T. Zuo, Y. Q. Cheng and P. K. Liaw, *Sci. Rep.* 3, 1455 (2013).
- [7] J. W. Yeh, S. K. Chen, S. J. Lin, J. Y. Gan, T. S. Chin, T. T. Shun, C. H. Tsau and S. Y. Chang, *Adv. Eng. Mater.* 6, 299 (2004).
- [8] C. L. Tracy, S. Park, D. R. Rittman, S. J. Zinkle, H. Bei, M. Lang, R. C. Ewing and W. L. Mao, *Nat. Comm.* 8, 15634 (2017).
- [9] D. B. Miracle and O. N. Senkov, *Acta materialia* 122, 448 (2017).
- [10] O. N. Senkov, G. B. Wilks, J. M. Scott and D. B. Miracle, *Intermetallics* 19, 698 (2011).
- [11] M. C. Tropicovsky, J. R. Morris, P. R. C. Kent, A. R. Lupini and G. M. Stocks, *Phys. Rev. X* 5, 011041 (2015).
- [12] J. -W. Yeh, *JOM* 65, 12 (2013).
- [13] J. Guo, H. Wang, F. von Rohr, Z. Wang, S. Cai, Y. Zhou, K. Yang, A. Li, S. Jiang, Q. Wu, R. J. Cava, and L. Sun, *Proc. Natl. Acad. Sci. USA*, 114, 13144 (2017).
- [14] P. Koželj, S. Vrtnik, A. Jelen, S. Jazbec, Z. Jagličić, S. Maiti, M. Feuerbacher, W. Steurer and J. Dolinšek, *Phys. Rev. Lett.* 113, 107001 (2014).
- [15] J. Wu, B. Liu, Y. Cui, Q. Zhu, G. Xiao, H. Wang S. Wu, G. Cao and Z. Ren, *Sci. China Mat.* 63, 823 (2020).
- [16] B. Liu, J. Wu, Y. Cui, Q. Zhu, G. Xiao, S. Wu, G. Cao and Z. Ren, *Scripta Materialia* 182, 109 (2020).
- [17] S. Marik, K. Motla, M. Varghese, K. P. Sajilesh, D. Singh, Y. Breard, P. Boullay and R. P. Singh, *Phys. Rev. Mat.* 3, 060602 (2019).
- [18] K. Stolze, F. A. Cevallos, T. Kong and R. J. Cava, *J. Mater. Chem. C* 6, 10441 (2018).
- [19] See Supplemental Material for Rietveld refinement considering elements are equally occupied on every Wyckoff position.
- [20] Y. Mizuguchi, Md. R. Kasem, and T. A. D. Matsuda, *Mat. Res. Lett.* 9, 141 (2021).
- [21] L. Sun and R. J. Cava, *Phys. Rev. Materials* 3, 090301 (2019).
- [22] J. Kitagawa, S. Hamamoto and N. Ishizu, *Metals* 10, 1078 (2020).
- [23] E. Bauer and M. Sigrist, *Non-centrosymmetric Superconductor: Introduction and Overview* (Heidelberg, Springer-Verlag 2012).
- [24] R. P. Singh, A. D. Hillier, B. Mazidian, J. Quintanilla, J. F. Annett, D. M. Paul, G. Balakrishnan and M. R. Lees, *Phys. Rev. Lett.* 112, 107002 (2014).
- [25] D. Singh, A. D. Hillier, A. Thamizhavel and R. P. Singh, *Phys. Rev. B* 94, 054515 (2016).
- [26] D. Singh, Sajilesh K. P., J. A. T. Barker, D. McK. Paul, A. D. Hillier and R. P. Singh, *Phys. Rev. B* 97, 100505(R) (2018).
- [27] S. K. Ghosh, M. Smidman, T. Shang, J. F. Annett, A. D. Hillier, J. Quintanilla and H. Yuan, *J. Phys.: Condens. Matter* 33, 033001 (2021).
- [28] A. D. Hillier, J. S. Lord, K. Ishida and C. Rogers, *Phil. Trans. R. Soc. A* 377, 20180064 (2019).
- [29] Rodriguez-Carajal, *Physica B* 192, 55 (1993).
- [30] F. O. von Rohr, M. J. Winiarski, J. Tao, T. Klimczuk and R. J. Cava, *Proc. Natl. Acad. Sci. U. S. A.* 113, E7144 (2016).
- [31] E. Helfand and N. R. Werthamer, *Phys. Rev.* 147, 288 (1966).
- [32] M. Clogston, *Phys. Rev. Lett.* 9, 266 (1962).
- [33] O. Prakash, A. Thamizhavel and S. Ramakrishnan, *supercond. Sci. Technol.* 28, 115012 (2015).
- [34] Y. Li, J. Garcia, G. Franco, J. Lu, K. Lu, B. Rong, B. Shafiq, N. Chen, Y. Liu, L. Liu, B. Song, Y. Wei, S. S. Johnson, Z. Luo and J. Feng, *J. Appl. Phys* 117, 213912 (2015).
- [35] W. L. McMillan, *Phys. Rev.* 167, 331 (1968).
- [36] T. Shang, G. M. Pang, C. Baines, W. B. Jiang, W. Xie, A. Wang, M. Medarde, E. Pomjakushina, M. Shi, J. Mesot, H. Q. Yuan and T. Shiroka, *Phys. Rev. B* 97, 020502(R) (2018).
- [37] R. Kubo and T. Toyabe, *Magnetic Resonance and Relaxation* (North-Holland, Amsterdam, 1967).
- [38] J. E. Sonier, J. H. Brewer and R. F. Kiefl, *Rev. Mod. Phys.* 72, 769 (2000).
- [39] E. H. Brandt, *Phys. Rev. B* 37, 2349 (1988).
- [40] M. Tinkham, *Introduction to Superconductivity* (McGraw-Hill, New York, 1996).
- [41] Y. J. Uemura, V. J. Emery, A. R. Moodenbaugh, M. Suenaga, D. C. Johnston, A. J. Jacobson, J. T. Lewandowski, J. H. Brewer, R. F. Kiefl, S. R. Kreitzman, G. M. Luke, T. Riseman, C. E. Stronach, W. J. Kossler, J. R. Kempston, X. H. Yu, D. Opie and H. E. Schone, *Phys. Rev. B* 38, 909 (1988).
- [42] Y. J. Uemura, G. M. Luke, B. J. Sternlieb, J. H. Brewer, J. F. Carolan, W. N. Hardy, R. Kadono, J. R. Kempston, R. F. Kiefl, S. R. Kreitzman, P. Mulhern, T. M. Riseman, D. L. Williams, B. X. Yang, S. Uchida, H. Takagi, J. Gopalakrishnan, A. W. Sleight, M. A. Subramanian, C. L. Chien, m. Z. Cieplak, G. Xiao, V. Y. Lee, B. W. Statt, C. E. Stronach, W. J. Kossler and X. H. Yu, *Phys. Rev. Lett.* 62, 2317 (1989).
- [43] Y. J. Uemura, L. P. Le, G. M. Luke, B. J. Sternlieb, W. D. Wu, J. H. Brewer, T. M. Riseman, C. L. Seaman, M. B. Maple, M. Ishikawa, D. G. Hinks, J. D. Jorgensen, G. Saito and H. Yamochi, *Phys. Rev. Lett.* 66, 2665 (1991).
- [44] J. A. T. Barker, B. D. Breen, R. Hanson, A. D. Hillier, M. R. Lees, G. Balakrishnan, D. McK. Paul and R. P. Singh, *Phys. Rev. B* 98, 104506 (2018).
- [45] C. S. Lue, H. F. Liu, C. N. Kuo, P. S. Shih, J.-Y. Lin, Y. K. Kuo, M. W. Chu, T.-L. Hung and Y. Y. Chen, *Supercond. Sci. Technol.* 26, 055011 (2013).
- [46] D. A. Mayoh, J. A. T. Barker, R. P. Singh, G. Balakrishnan, D. McK. Paul and M. R. Lees, *Phys. Rev. B* 96, 064521 (2017).
- [47] S. Sundar, S. Salem-Sugui Jr., M. K. Chattopadhyay, S. B. Roy, L. S. Sharath Chandra, L. F. Cohen and L. Ghivelder, *Supercond. Sci. Technol.* 32 055003 (2018).
- [48] DOI :10.5286/ISIS.E.RB1920420